Bias-Dependent Generation and Quenching of Defects in Pentacene

D. V. Lang,[1,2] X. Chi,[2] T. Siegrist,[3] A. M. Sergent,[3] and A. P. Ramirez[3,2]
[1]*Los Alamos National Laboratory, Los Alamos, New Mexico 87545, USA*
[2]*Columbia University, New York, New York 10027, USA*
[3]*Bell Laboratories, Lucent Technologies, 600 Mountain Avenue, Murray Hill, New Jersey 07974, USA*
(Received 17 December 2003; published 13 August 2004)

We describe a defect generation phenomenon that is new to organic semiconductors. A defect in pentacene single crystals can be created by bias-stress and persists at room temperature for an hour in the dark but only seconds with 420 nm illumination. The defect gives rise to a hole trap at $E_v + 0.38$ eV and causes metastable transport effects at room temperature. Creation and decay rates of the hole trap have a 0.67 eV activation energy with a small (10^8 s^{-1}) prefactor, suggesting that atomic motion plays a key role in the generation and quenching process.

DOI: 10.1103/PhysRevLett.93.076601 PACS numbers: 72.80.Le, 85.65.+h

Defects and impurities play a dominant role in determining the properties of semiconductors. In the emerging area of organic semiconductors, however, little is known about them. One of the few known examples is tetracene as an impurity in anthracene, which forms a 0.42 eV hole trap [1,2]. Deep-level transient spectroscopy (DLTS) measurements of poly(*p*-phenylene-vinylene) (PPV) films [3] and polycrystalline pentacene films [4] indicate the presence of deep gap states. Calculations show that point defects in anthracene should give a trap level of about 0.28 eV and dislocations should give a level of about 0.2 eV [2,5]. Northrup and Chabinyc [6] have recently calculated the gap state energies of various hydrogen- and oxygen-induced defects in crystalline pentacene and find hole traps at 0.34 and 0.18 eV from the valence band, respectively. They propose that these defects can be formed by bias-stress and could potentially explain the metastable bias-stress effects in pentacene thin film transistors (TFTs) reported by Knipp *et al.* [7]. Reynolds *et al.* [8] have also made passing reference to metastable effects, such as persistent photoconductivity, in pentacene thin films.

In this Letter we report a room-temperature defect creation phenomenon that is new to organic semiconductors. We observe a defect in pentacene single crystals that can be generated by bias-stress and exhibits metastable effects in space-charge-limited current (SCLC) IV curves. The defect concentration recovers to zero-field equilibrium at room temperature in the dark in more than an hour, but in less than 1 s if illuminated with photons above the band gap (2.2 eV [9]). Defect reactions of this type have been observed in inorganic semiconductors [10], but at significantly higher temperatures or with optical excitation. Our observation of such phenomena at room temperature implies that the energies of defect creation and/or motion are smaller in organic semiconductors compared to inorganic semiconductors. This is plausible given the weak intermolecular bonding and the calculations of Northrup and Chabinyc [6], who show that defects in aromatic molecular solids can be readily formed by the addition of H or OH to disrupt the π electron system. Hence, the phenomenon that we observe is likely to occur in other aromatic molecular semiconductors besides pentacene, and offers possible routes to improving the mobility in these materials.

The pentacene crystals were grown by physical vapor transport as described previously [11] and were 10–30 mm^2 in area and 25–50 μm thick. To evaluate crystal quality, rocking curves of a sample from the same batch as the transport sample were obtained on a custom four-circle diffractometer with monochromated Cu-$K\alpha$ radiation. Rocking curves of (002) and (004) reflections were evaluated, and the widths indicated mosaic spreads of the order of 0.2 degrees and better. The contacts were formed by evaporating 5 nm of Ti followed by 500 nm of Au in an *e*-beam evaporator through a shadow mask giving an array of 400 μm-square metal pads separated by 30 μm gaps along the columns and 108 μm gaps along the rows. The measurements reported in this paper were made on the 30 μm gaps, which had a specular surface and were in the triclinic *ab* plane of the crystal. There were no obvious crystal defects, domain walls, or grain boundaries in the measured gaps. The samples were mounted in a temperature-variable vacuum probe station and measured with a Keithley 6517A electrometer. Photoexcitation was with a grating monochromator focused to an optical flux of 3×10^{13} photons/cm^2 sec at 420 nm (2.95 eV).

Figure 1 shows the SCLC IV curves under various conditions. The initial condition for the dotted lines in Fig. 1 is the zero-field equilibrium state, which may be achieved in the dark at zero bias in several hours at room temperature, or more rapidly at 360 K in 1 min or with 2.95 eV photons at room temperature in a few seconds. In Fig. 1 we used 2.95 eV photons. All IV curves were from $V = 0$ to a particular end-point voltage (30, 100, 300, or 600 V) and consisted of 20 evenly spaced bias steps with a 5 sec dwell time. The initial scans define a typical SCLC

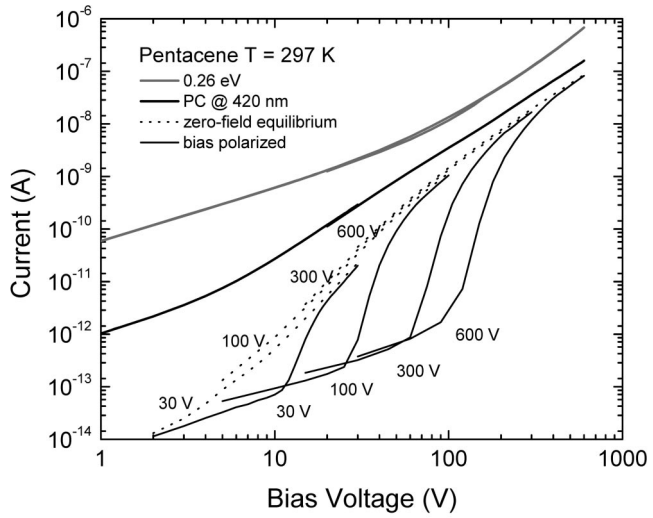

FIG. 1. Space-charge limited current (SCLC) versus bias voltage showing metastable bias-polarization effects for four voltages (30, 100, 300, and 600 V). The additional two curves are 420 nm photoconductivity for the same contact location and SCLC for a different location with a 0.26 eV activation energy. The latter two curves show no hysteresis.

power law ($I \sim V^n$) [2,12] with an initial exponent $n = 3.5$ and an asymptotic exponent $n = 2$ at high bias. Such a power law for $n > 2$ is indicative of an exponential distribution of traps with a characteristic energy of $(n - 1)$kT, where k is the Boltzmann constant and T is the absolute temperature.

The initial condition for the solid lines in Fig. 1 is a bias-polarized state, which is achieved by holding the sample at the respective end-point voltage for 100 sec. Each of the polarized scans was from $V = 0$ to the respective end-point voltage after the polarization voltage was removed. Subsequent scans repeated within a few minutes of the polarized scan, but without additional polarization, behave the same as the first and are independent of the bias scan direction. All of the polarized IV curves in Fig. 1 have similar shapes—a polarization-dependent voltage threshold and a steep power-law ($n = 11$) increase in current that asymptotically joins the initial curve at the polarization bias. These bias-polarized curves display the classic shape of SCLC IV curves in material with traps [2,12,13] where the steady-state current changes rapidly as the Fermi level moves through a trap level as a function of bias voltage. The voltage threshold is a measure of the trap concentration, while the trap energy can be inferred from the activation energies of the current above and below the current step. For the 600 V bias-polarized state, the activation energy is 0.55 eV below the step and 0.21 eV at 600 V after the step. If we take the activation energy to be approximately equal to the Fermi level, the 0.38 eV midpoint corresponds to the center of the band of traps. The trap concentration can be calculated [12,13] from the voltage threshold (100 V), trap energy (0.38 eV), and power law ($n = 11$) to be 2.5×10^{14} cm^{-3} for a 0.1 eV-wide distribution of trap energies. This is close to the maximum uniform space-charge density (5×10^{14} cm^{-3}) that can be supported in such a structure at 600 V [14]. Thus, the bias-polarized state corresponds to an increased concentration of defects with gap states centered at $E_v + 0.38$ eV, while the zero-field equilibrium state corresponds to the disappearance of these defects.

The trap dominated SCLC curves are only found, however, in the regions of our crystals where the low-field Fermi level is more than 0.4 eV from the valence band so that the Fermi level can be swept through the trap level with increasing bias. Parts of our crystals have a Fermi level as low as 0.26 eV where the IV step due to trap filling cannot be observed and there is no hysteresis in the IV curves, as shown in Fig. 1. The spatial distribution of Fermi levels results from unintended variations in p-type dopants across our crystals. The metastable curves in Fig. 1 also exhibit nonhysteretic conductivity when illuminated at 420 nm; this photoconductivity also has an activation energy of 0.26 eV.

We can study the dynamics of the transition between the bias-polarized state and the low-field equilibrium state by measuring current versus time at a fixed bias following different initial conditions. To optimize the dynamic range and signal-to-noise ratio, we have studied the initial buildup in the 600 V bias-polarized state and the decay of this state at 140 V. The decay transients for three temperatures (320, 340, and 360 K) in Fig. 2(a) are measured at 140 V immediately after 1000 s at 600 V and correspond to the transition from the 600 V-polarized state to the 140 V equilibrium state. The crosses on the decay curves in Fig. 2(a) denote the shift with temperature for the same relative point on each curve and are shown in the Arrhenius plot in Fig. 3. The polarization transients for three temperatures (300, 320, and 340 K) in Fig. 2(b) are measured at 600 V (2×10^5 V/cm) immediately after the end of the decay transient at 140 V and correspond to the transition from the 140 V equilibrium state to the 600 V bias-polarized state. The open circles on these curves denote the inflection point that changes with temperature and are shown in Fig. 3. The current versus time during bias-polarization has the same shape for other polarization voltages; thus the transition rate to the bias-polarized state does not depend on the magnitude of the electric field.

The temperature dependence of the transitions between the two limiting states is shown in Fig. 3. We have plotted the inverse of the times marked in Figs. 2(a) and 2(b) as the transition rate in the figure. These data are fit with a function of the form $r = A \exp(-E/\mathrm{kT})$, where r is the transition rate, A is the exponential prefactor, and E is the activation energy. The decay rate in Fig. 3 has $E = 0.67$ eV and $A = 9.0 \times 10^7$ s^{-1} while the polarization

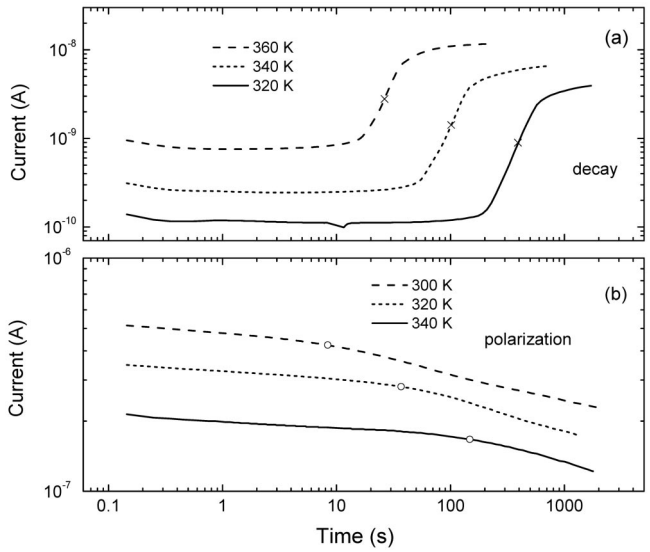

FIG. 2. Current versus time at fixed bias for different initial conditions and temperatures. (a) Decay of the 600 V bias-polarized state at 140 V for three temperatures. The cross marks on the curves are at the same fraction of the respective maxima and form the basis for the decay points in Fig. 3. (b) Buildup of the 600 V bias-polarized state at 600 V after equilibrium at 140 V for three temperatures. The open circles on the curves are at the intersection of power-law fits for short and long times and form the basis for the polarization points in Fig. 3.

rate has $E = 0.67$ eV and $A = 1.05 \times 10^9$ s^{-1}. The transitions in Figs. 2(a) and 2(b) are broader than a single exponential time constant, however, and correspond to a distribution of rates. The energies and prefactors in Fig. 3 roughly characterize the center of this distribution. Note that the activation energies for the decay and polarization rates are the same. If the metastable effects were due to the trapping and thermal release of holes at defect states in the gap, these energies would not be the same. Equal barriers for both directions of a reaction imply that the equilibrium energies of the final states are the same. This is true for two-level systems or atomic motion, but we are not aware of examples related to carrier trapping. Note also that the exponential prefactors are unusually small for thermal capture and emission of carriers at traps; the factor for the decay rate is 10^4smaller than the more typical trap emission prefactor of 10^{12} s^{-1} [15].

Our results suggest a model where defects are created when the Fermi level is less than 0.3 eV from the valence band and are quenched either thermally or optically when the Fermi level is more than 0.4 eV from the valence band. The same 0.67 eV activation energy for the defect generation and quenching process, along with the low (10^8 s^{-1}) prefactor, is consistent with a model where the rate-limiting step is the diffusion of weakly bound atoms. Our SCLC results could also be explained by a metastable electrostatic barrier in the sample created by defects that are positively charged by hole capture at the polarization bias, such as at a grain boundary [16]. However, the lack of electric field dependence of our observed polarization rate rules out such a model. A large lattice relaxation model [17] is also unlikely considering the weak van der Waals bonding of the molecular crystal and the fact that intramolecular distortions are unlikely to give 0.67 eV energy barriers [6]. Therefore, we believe that models involving carrier trapping and a metastable electrostatic barrier cannot describe our data.

On the other hand, we believe the pentacene defect reaction scenario proposed by Northrup and Chabinyc [6] gives important clues about the origin of our effect. This model is based on density functional calculations of various hydrogen- and oxygen-induced defects in crystalline pentacene. Adding H or OH to a pentacene molecule ($C_{22}H_{14}$) forms a fourfold-coordinated C atom (a C-H_2 defect) that gives rise to three charge states in the gap ($+/0/-$). The capture and emission transitions among these states correspond to a deep donor level ($+/0$) at $E_v + 0.34$ eV and a deep acceptor level ($0/-$) at $E_v + 0.8$ eV. A pentacene molecule with two C-H_2 defects is dihydropentacene ($C_{22}H_{16}$), which is more stable than $C_{22}H_{15}$ and has no states in the gap. Therefore, the reaction

$$2h^+ + C_{22}H_{16} + C_{22}H_{14} \rightarrow (C_{22}H_{15})^+ \qquad (1)$$

is driven to the right as the Fermi level drops below $E_v + 0.34$ eV where the pairing energy is given by 1.04–2(0.34–E_F) eV, with the Fermi energy E_F measured from the valence band. For 600 V in our experiments $E_F = 0.21$ eV so the pairing energy reduces to 0.78 eV.

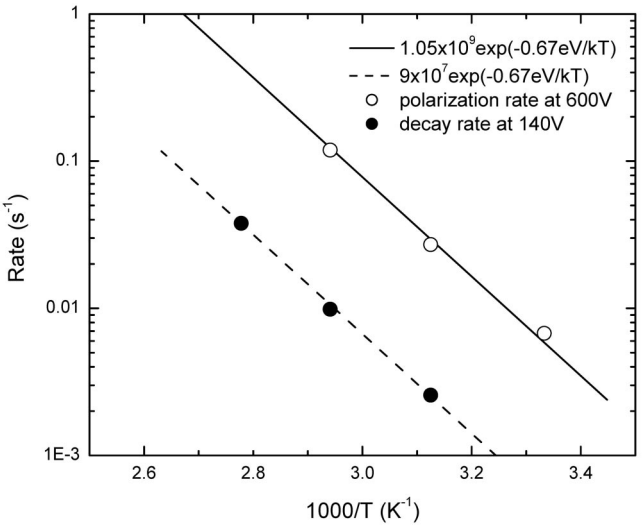

FIG. 3. Transition rate versus inverse temperature for the decay and polarization data in Fig. 2. The fits to these data indicate the activation energy and exponential prefactor for each process.

Our observed range of defect energies ($E_v + 0.38 \pm 0.05$ eV) is extremely close to the calculated energy ($E_v + 0.34$ eV) of the C-H_2 defect. In addition, the Fermi level dependence of our defect creation effect is remarkably close to the calculated energy of the positive charge state of the C-H_2 defect. Namely, we see no polarization hysteresis unless the Fermi level can be reduced below 0.3 eV by the applied bias to create defects and returned above 0.4 eV at low bias to observe the decay of the defect. However, the simple C-H_2 defect reaction in Eq. (1) cannot adequately explain our 0.67 eV activation barriers and the low exponential prefactors. Northrup and Chabinyc envision a model in Eq. (1) where the C-H_2 defect is created by a proton jumping from a dihydropentacene molecule to a neighboring pentacene. This would not give the symmetric generation and quenching activation energies that we observe because the equilibrium energies of the two sides of Eq. (1) are very different. However, if the rate-limiting step in the process were the thermally activated diffusion of H, we would see symmetric barriers. In fact, activation energies below 1 eV are typical of interstitial diffusion of impurities in inorganic semiconductors [18]. If the mobile H moves some distance before finding a suitable reaction site, the prefactor is of order 10^{12} s^{-1} for each hop divided by the average number of hops. Since the observed prefactors are in the range 10^8–10^9 s^{-1}, the average distance traveled is the square root of the number of hops (10^3 to 10^4) times the distance of a single hop (assume $\sim$5 Å), which is approximately 30 nm and corresponds to a reaction site concentration of order 5×10^{16} cm^{-3}.

Finally, we need to explain the rapid quenching of our defects by above–band-gap light. The quenching conditions in our experiments correspond to C-H_2 defects being in the neutral charge state before illumination. The capture of a photo-generated electron into the $E_v + 0.8$ eV level of C-H_2 from the conduction band must dissipate 1.4 eV, which is larger than the diffusion barrier of 0.67 eV. If the electronic capture energy were channeled into the appropriate reaction coordinate by the well-known mechanism of recombination-enhanced diffusion [10,19], this could lead to the greatly enhanced reaction rate we observe. We must stress, however, that this is merely a conjecture and the actual mechanism for the rapid photoquenching of the defects is presently unknown.

In summary, we have described a bias-dependent defect generation and quenching effect in pentacene single crystals that gives rise to metastable transport effects at room temperature. Space-charge limited current measurements in the bias-polarized state indicate an increase in the concentration of hole traps centered at $E_v + 0.38$ eV that persist for nearly an hour in the dark but can be rapidly removed by light above the 2.2 eV band gap. The creation and decay rates of this trap have the same activation energy (0.67 eV) with a small exponential prefactor that is typical of atomic diffusion. Some aspects of our results can be explained by the dissociation of C-H_2 defect pairs, as proposed by Northrup and Chabinyc, but a detailed explanation of our results must take into account the apparent atomic diffusion that we observe. Our results suggest that fourfold coordinated C atoms with associated intermolecular H diffusion may be an important class of defect reactions in pentacene and, perhaps, other organic solids as well.

We wish to acknowledge stimulating discussions with M. S. Hybertsen and M. L. Steigerwald. This work was funded through the DOE Basic Energy Sciences Division, Nanoscience Engineering and Technology program, FWP 04SCPE389, by the Nanoscale Science and Engineering Initiative of the National Science Foundation under NSF Contract No. CHE-0117752 and by the New York State Office of Science, Technology, and Academic Research (NYSTAR).

[1] N. Karl *et al.*, J. Vac. Sci. Technol. A **17**, 2318 (1999).
[2] M. Pope and C. E. Swenberg, *Electronic Processes in Organic Crystals and Polymers* (Oxford, New York, 1999).
[3] A. J. Campbell *et al.*, Synth. Met. **111**, 273 (2000).
[4] Y. S. Yang *et al.*, Appl. Phys. Lett. **80**, 1595 (2002).
[5] J. Sworakowski, Mol. Cryst. Liq. Cryst. **33**, 83 (1976).
[6] J. E. Northrup and M. L. Chabinyc, Phys. Rev. B **68**, 041202 (2003).
[7] D. Knipp *et al.*, J. Appl. Phys. **93**, 347 (2003).
[8] S. Reynolds *et al.*, J. Non-Cryst. Solids **266–269**, 994 (2000).
[9] E. A. Silinsh *et al.*, Phys. Status Solidi (a) **25**, 339 (1974).
[10] D. V. Lang, Annu. Rev. Mater. Sci. **12**, 377 (1982).
[11] V. Y. Butko *et al.*, Appl. Phys. Lett. **83** 4773 (2003).
[12] M. A. Lampert and P. Mark, *Current Injection in Solids* (Academic Press, New York, 1970).
[13] P. W. M. Blom, M. J. M. de Jong, and J. J. M. Vleggaar, Appl. Phys. Lett. **68**, 3308 (1996).
[14] S. M. Sze, *Physics of Semiconductor Devices* (Wiley, New York, 1981).
[15] D. V. Lang, J. Appl. Phys. **45**, 3023 (1974).
[16] C. H. Seager and T. G . Castner, J. Appl. Phys. **49**, 3879 (1978).
[17] D. V. Lang and R. A. Logan, Phys. Rev. Lett. **39**, 635 (1977).
[18] A. G. Milnes, *Deep Impurities in Semiconductors* (Wiley, New York, 1973).
[19] D. V. Lang and L. C. Kimerling, Phys. Rev. Lett. **33**, 489 (1974).